RSC Advances

PAPER

View Article Online
View Journal | View Issue

Cite this: *RSC Adv.*, 2025, **15**, 28581

Tailoring cell behaviour by surface micropatterning and interconnected porous structure of gelatin/nano-silica/PLGA 3D composite scaffold for bone tissue engineering

Nur Rofiqoh Eviana Putri, *[a] Huajian Chen,[b] Naoki Kawazoe,[b] Felicity R. A. J. Rose,[c] Ricky D. Wildman[d] and Guoping Chen *[b]

Scaffold architecture with complementary features on the surface brings the desired properties in the surface chemistry. That structure plays a critical role in tissue engineering to tailor cell behaviour and promote effective transport for cell growth and tissue regeneration. In this work, a controllable interconnected three-dimensional (3D) porous scaffold with surface micropatterning was fabricated. Nozzle-based Aerojet dispenser 3D printing was used to form printed ice as a fugitive ink combined with a freeze-drying method of gelatin/nano-silica/poly lactic-*co*-glycolic acid (PLGA) and ice particulates to fabricate a composite scaffold with supporting properties. Several designs of printed ice were explored and the HUVECs' behavior on different surface patterns was analyzed. The results showed that HUVECs exhibited orientation adhesion and growth with a certain direction after 6 days of culture. The 3D-controlled interconnected porous scaffolds with surface micropatterning then were used for the 3D culture of hMSCs. The hMSCs analysis showed a facilitating effect for cell distribution and growth in the 3D composite scaffolds compared to the control scaffold without interconnected porous structure and surface micropatterning. This study demonstrated that controlled cell behavior by patterning the surface of the scaffold and improved cell growth by controlling the interconnected inner porous scaffold has a significant role in bone tissue engineering.

Received 25th April 2025
Accepted 1st August 2025

DOI: 10.1039/d5ra02891d

rsc.li/rsc-advances

1 Introduction

Bone regeneration is a very complex process that needs two crucial factors, *i.e.* blood supply to the defect and fixation stability (biomechanics).[1] It follows the bone healing cascade including the inflammatory (hematoma formation to promote angiogenesis), reparative (bone callus formation), and bone remodeling process.[2,3] The bone regeneration cascade is useful for small defects (less than 2 cm) because it is a highly vascular tissue. In a large defect, it is still difficult for the bone tissue to repair and regenerate by itself. That leads to permanent bone defects and loss of function.[4] Therefore, clinical treatment is needed for further regeneration to initiate the inflammatory steps in the initial bone regeneration cascade due to the lack of features for the transport process.

The field of tissue engineering, which focuses on regenerating tissue defects by using a combination of cells, growth factors, and scaffolds offers great advantages for bone treatment.[5] Tailoring the scaffold architecture with supporting features is essential to promote the transport of essential molecules (oxygen, glucose, and amino acids) and eliminate the by-products of the degradation process. Cells within the body are located in no more than 100 μm of vascular channels.[6,7] Without the interconnected porous structure, nutrient transport is dependent only on diffusion, which is only efficient for short depths. Thus, in large scaffolds, the penetration of nutrients occurs on the surface, leading to cell death at the hypoxic core. It triggers the inflammatory responses and rejection of the native tissues and cannot form an excellent integration with the host tissue.[8]

Besides the interconnected pores inside the bulk of the scaffold, the surface properties also perform a critical role in the cell attachments, migration, and proliferation as well as the adsorption of bioactive molecules, which leads to successful tissue regeneration.[9,10] Several strategies have been developed to create a scaffold with surface patterning such as lyophilization

[a]*Department of Chemical Engineering, Faculty of Engineering, Universitas Gadjah Mada, Jl. Grafika No 2, Kampus UGM, Yogyakarta, 55284, Indonesia. E-mail: nur.rofiqoh.e@ugm.ac.id*

[b]*Research Center for Macromolecules and Biomaterials, National Institute for Materials Science, 1-1 Namiki, Tsukuba, Ibaraki, 305-0044, Japan. E-mail: Guoping.CHEN@nims.go.jp*

[c]*Biodiscovery Institute, School of Pharmacy, University of Nottingham, Nottingham, NG7 2RD, UK*

[d]*Centre for Additive Manufacturing, Faculty of Engineering, University of Nottingham, Nottingham, NG7 2RD, UK*

and molding techniques,[10] phase separation micro-molding process,[11] electrospinning and molding techniques,[12] and electron beam lithography.[13] They can align customized networks and patterning using a broad range of materials, simple processes, and low cost. However, they have limitations in achieving a complex structure, especially for 3D construct fabrication.

Previously developed scaffolds were prepared by combined the surface patterning and porous bulk scaffold to face those challenges. The work by Guicai Li, *et al.* demonstrated the fabrication of a micropatterned scaffold to guide the endothelial cell alignment by using a PDMS stamp for casting the chitosan surface patterning and lyophilization to form the porous structure on the bulk of the scaffold. However, it lacked controlled internal porosity, which is essential for effective nutrient diffusion.[14] Additionally, Maria Moffa, *et al.* presented combined micro- and nano-topographic cues including the grooved micropatterns and electrospun fibers to guide the endothelial cell alignment. However, their approach lacked variation in the surface patterns.[12]

In order to solve those problems, this work combined the use of additive manufacturing also known as 3D printing with the ice particulates/freeze drying method to form a 3D scaffold with controlled interconnected inner porous structures and surface micropatterning. The surface pattern of the scaffold could regulate the endothelial cell behaviour, meanwhile the interconnected pores on the bulk of the scaffold could enhance nutrient transport and cell penetration. In order to form a micropatterned surface scaffold, Aerojet dispenser 3D printing was used to print water onto a frozen substrate with the prepared design. The Aerojet dispenser can offer great flexibility for more complex pattern formation with biocompatibility. Shangwu Chen, *et al.* used the Aerojet dispenser for microgrooved collagen porous scaffold fabrication to engineer skeletal muscle tissue.[15] They successfully controlled the alignment of myoblasts, which resulted in the synthesis of muscle extracellular matrix. However, they have not explored different patterns besides the microgroove yet and did not control the interconnected porous scaffolds. Another study was conducted by Ying Chen, *et al.* by fabricating the composite scaffold of dexamethasone-loaded calcium phosphate nanoparticle/collagen with a microgroove network.[16] They presented promotive effects for angiogenesis and osteogenesis on the micro-grooved composite scaffold compared to the control scaffold. However, they have not studied the different patterns that potentially affect the HUVECs' alignment and orientation. Therefore, in this work, we explored the formation of different patterning and optimized the parameters during printing to form the high-resolution and stable printed ice.

Bioactive silica is selected as one of the materials for scaffold fabrication since provides biomineralization capability.[17] The use of nano-silica for scaffolds increased protein adsorption and controlled swelling ability. It was also biodegradable and improved apatite deposition.[18] However, silica scaffolds have low formability and high brittleness, so gelatin and PLGA were added to improve the stiffness and mechanical properties.[19] In addition, gelatin has a similar composition to collagen and excellent biocompatibility, which is often used for the regeneration of bones and cartilage.[20] Meanwhile, the PLGA has controllable mechanical properties, which could improve the strength and stability of the composite material.[21] Finally, the 3D construct of scaffolds with surface patterned and controlled interconnected porous structures of gelatin/nano-silica/PLGA composite scaffolds were explored.

2 Materials and methods

2.1 Exploration of 3D-printed ice

Frozen 3D-printed ice was used as sacrificial ink to form different patterns on the surface of the scaffold. The 3D printing of water onto frozen substrate was done using a jet dispenser (MJEY-3-CTR, Musashi Engineering Inc), which was controlled by a SHOT mini 200α (Musashi Engineering Inc). A different pattern was prepared by inputting the program on the SHOT mini 200α to control the movement of X, Y, and Z directions. Perfluoro alkoxy film (PFA film, Universal Co., Ltd) was wrapped on a copper plate, which was then frozen by liquid nitrogen. Ultrapure water was filled on the syringe and ejected through a 0.140 mm nozzle by applying the air pressure, that was connected to the jet dispenser. The water droplets were immediately frozen and formed the pre-prepared pattern of frozen printed ice.

The fixed parameters during printing were a printing speed of 40 mm s^{-1}, on time (time of water being held at the edge of the nozzle) of 3 ms, number of layers of 4, and a nozzle diameter of 0.14 mm. Meanwhile, some parameters were varied including the off time (interval time between the water droplet), and air pressure. The printed line pattern was captured using an Olympus microscope with a DP22 camera so that the line width and line gap of the printed line can be measured using ImageJ software (ImageJ2, NIH) on 4 images of each varied parameter.

2.2 Fabrication of porous gelatin scaffold with different surface patterns

A porous scaffold with a different surface pattern (Scheme 1(A)) was prepared by using the printed ice to control the surface pattern and a mixture of gelatin with ice particulates to form the porous scaffold after the freeze-drying process. The printed ice was prepared as described before using optimum printing conditions, *i.e.*, the printing speed of 40 mm s^{-1}, on time of 3 ms, nozzle diameter of 0.14 mm, off time of 9 ms, air pressure of 0.006 MPa, and number of layers of 4. On the other hand, the ice particulates were prepared by spraying Milli-Q water into liquid nitrogen using a sprayer. They were then sieved by sieves with mesh pores sizes of 150 and 250 μm to control the diameter of ice particulates. The sieving process was performed in the low-temperature chamber (ESPEC, Osaka, Japan) at −15 °C.

Gelatin solution at 4.0 (w/v)% was prepared by adding the gelatin granules (porcine-derived gelatin, Nitta Gelatin, Inc.) into 30.0 (v/v)% acetic acid as the solvent. It was stirred at 45 °C for 2 hours and then continued stirring at room temperature for 1 hour. The acetic acid solution was used as a solvent to reduce the gelation of the gelatin solution at low temperatures. All pre-

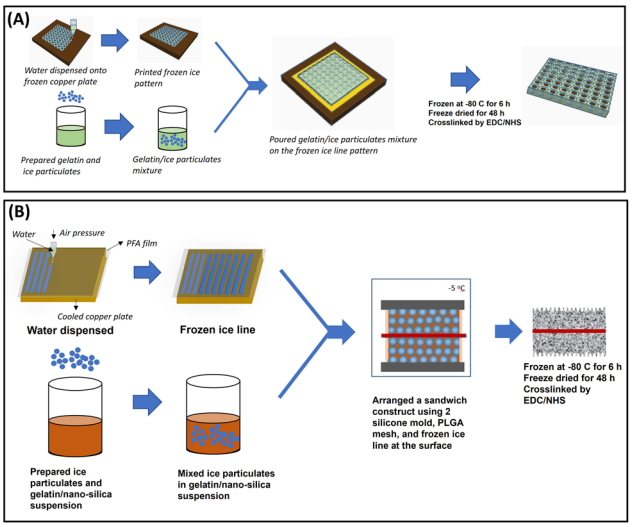

Scheme 1 Schematic preparation of (A) scaffold with different surface patterns, and (B) 3D sandwich scaffold with patterned surface and interconnected porous structure.

prepared ice particulates, frozen printed ice, gelatin, and tools were kept at −5 °C for 2 hours to allow temperature balance prior to assembly.

The ice particulates were added into 4.0 (w/v)% gelatin solution with the ratio of ice particulates/gelatin solution of 70 : 30 (w/v) and thoroughly mixed until homogeneous. In order to control the thickness of the scaffold, a 1 mm thick silicone mold was placed onto frozen printed ice. The mixture of ice particulates/gelatin was then poured onto the silicone mold, flattened with a steel spatula and then covered with a glass plate. It was moved and kept at −80 °C freezer for at least 6 hours to ensure complete freezing. The frozen construct was detached from the glass plate and then freeze-dried for 48 hours.

2.3 Fabrication of gelatin/nano-silica/PLGA 3D composite scaffolds with patterned surface and interconnected porous structure

Scaffolds were prepared by frozen printed ice, ice particulates, vicryl knitted mesh of polyactin 910 (a 90 : 10 copolymer of glycolic acid and lactic acid (PLGA) Ethicon, Inc., Somerville, NJ) mesh, nano-silica, and gelatin solution. The schematic fabrication is shown in Scheme 1(B). First, an 8.0 (w/v)% gelatin solution was added to a 2.0 (v/v)% nano-silica suspension to prepare a gelatin/nano-silica mixture with the final concentration of 4.0 (w/v)% gelatin and 1.0 (v/v)% nano-silica in 35.0 (v/v)% acetic acid. It was stirred at room temperature for 1 hour to form a homogeneous mixture. The materials and tools were then kept in a −5 °C low-temperature chamber for 2 hours to balance the temperature. Subsequently, a 1 mm thick silicone mold was placed onto frozen printed ice, which was prepared above the PFA-wrapped copper plate. A mixture of ice particulates/gelatin/nano-silica with a ratio of ice particulates and gelatin/nano-silica mixture of 70 : 30 (w/v) was poured onto frozen printed ice with the silicone mold. The surface of the mixture was flattened with a steel spatula and covered with a knitted PLGA mesh, which was then immersed in a gelatin solution. Another 1 mm thick silicone mold was placed onto the construct and then poured with another mixture of ice particulates/gelatin/nano-silica. The surface of the mixture was flattened with a spatula and covered with frozen printed ice. After mixing, the construct was moved into a −80 °C freezer and kept for at least 6 hours to ensure complete freezing then freeze-dried for 48 hours. As a control, a scaffold was prepared without the frozen printed ice on the surface, nano-silica, and ice particulates on the matrix.

2.4 Crosslinking of scaffolds

Chemical crosslinking using 50 mM 1-ethyl-3-(3-dimethylaminopropyl) carbodiimide (EDC, Peptide Institute, Inc), 20 mM *N*-hydroxysuccinimide (NHS, Wako Pure Chemical Industries, Ltd) and 0.1(w/v)% 2-(*N*-morpholino) ethanesulfonic acid (MES) in three solvents of decreasing ethanol concentrations with ratio of ethanol/water of 95/5, 90/10 and 85/15 (v/v). After the freeze drying, the scaffold was immersed in pure ethanol by degassing, followed by soaking in the first crosslinking solution (ethanol/water 95/5) for 8 hours, the second solution (ethanol/water 90/10) for 8 hours, and then the third solution (ethanol/water 85/15) for 8 hours. To remove the unreacted reagents, the scaffold was then rinsed with MiliQ water 10 times at room temperature and re-freeze dried for 48 hours to get the final crosslinked scaffold.

2.5 Characterization of scaffolds

The morphology of scaffolds was analyzed by a JSM-5610 Scanning Electron Microscope (SEM; JEOL, Tokyo, Japan). The surface, horizontal, and vertical cross-sections of scaffolds were sputter-coated with gold before characterization. Samples were observed at a 10 kV acceleration voltage and the pore size of the scaffold was calculated using four SEM images of each type of scaffold by measuring the diameters of pores using ImageJ software (ImageJ2, NIH).

For porosity measurement, the scaffolds were punched using a biopsy punch with a diameter size of 6 mm. The calculation was conducted by measuring the weight of water filling the void spaces in the scaffolds using the following equations:[22,23]

$$\text{Porosity} = \frac{V_{\text{pore}}}{V} \times 100\% = \frac{W_2 - W_1}{\rho V} \times 100\% \quad (1)$$

where V_{pore} is the pores volume, V is the scaffold volume, W_1 is the weight of the dry scaffold, W_2 is the weight of the hydrated scaffold with water, and ρ is the density of water. Triplicate samples were used for the measurements.

2.6 *In vitro* cell culture of HUVECs onto different surface patterns of porous scaffold

HUVECs (C2519A, Lonza) were used for the *in vitro* cell culture on the scaffolds with different surface patterns. Before cell seeding, the scaffolds were punched into cylindrical discs (Φ10 mm × H 1 mm) and then sterilized by immersing them in ethanol for 1

hour. They were washed with PBS 5 times and then immersed in DMEM medium for at least 2 hours. The HUVECs were sub-cultured using endothelial cell growth medium (EGM2, CC-3162, Lonza) that contained EGM2 Single Quots (CC-4176, Lonza). After reaching confluence, the cells were harvested using trypsin/EDTA and then re-suspended in DMEM to prepare a cell suspension solution with the density of 2×10^6 cells per mL for cell seeding. 90 μL of the HUVECs suspension solution was dropped on the sterilized scaffold and incubated for 3 hours to provide the cells attachment. After 3 hours, the glass ring with a diameter of 10 mm, which was placed on the scaffold to provide the cell seeding was removed, and then DMEM low glucose medium supplemented with 10 mM β-glycerophosphate and 100 nM dexamethasone (Dex) was added into scaffold disc. The medium also contained 10% fetal bovine serum, 4 mM glutamine, 100 U ml^{-1} penicillin, 100 μg ml^{-1} streptomycin, 0.1 mM nonessential amino acids, 0.4 mM proline, 1 mM sodium pyruvate and 50 μg ml^{-1} ascorbic acid. Seeded samples were incubated in a humidified incubator at 37 °C and 5% CO_2 with the medium being changed every 3 days (Scheme 2(A)).

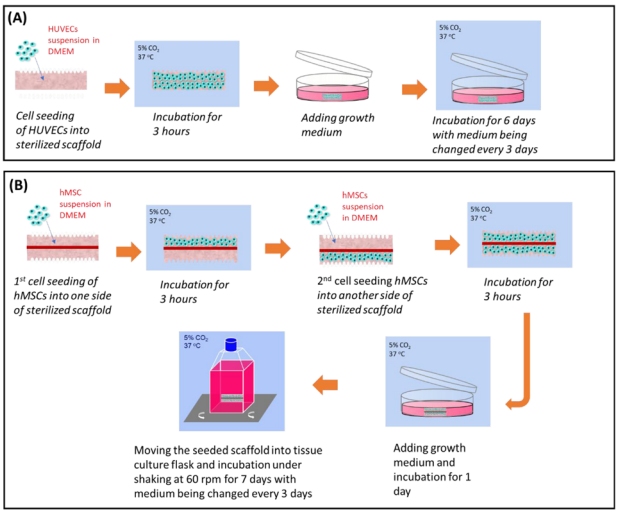

Scheme 2 Schematic *in vitro* cell culture of (A) HUVECs on the scaffold with different surface patterns, and (B) hMSC on the 3D sandwich composite scaffold with patterned surface and interconnected porous structure.

2.7 *In vitro* cell culture of hMSCs onto a 3D composite scaffold with patterned surface and interconnected porous structure

3D composite scaffolds were punched into cylindrical discs with a diameter of 6 mm and then sterilized by immersion in ethanol followed by washing with PBS 5 times. The hMSCs (passage 4, Lonza) were sub-cultured using MSCBM medium (Lonza) until reached confluence. They were then harvested using trypsin/EDTA and re-suspended in DMEM to obtain a cell suspension solution of 2×10^6 cells per mL. 80 μl of hMSCs suspension solution was seeded onto one side of the scaffolds and cultured at 37 °C for 3 h. After that, the scaffolds were turned upside down and another 80 μl of hMSCs suspension solution was seeded. They were then cultured at 37 °C for 3 h to allow cell attachment and fresh culture medium was added. After 1 day, the seeded scaffolds were moved to a 75 cm^2 tissue culture flask and cultured under shaking at 60 rpm with the medium being changed every 3 days (Scheme 2(B)).

2.8 Cell characterization

After 1 day of culture, cell adhesion and distribution in the 3D composite sandwich scaffolds were analyzed by SEM. Samples were rinsed with PBS and fixed with 2.5% glutaraldehyde at room temperature for 1 hour. After that, they were washed with PBS and water respectively, and were freeze-dried for 48 hours. Before the analysis, the surface, horizontal cross-section, and vertical cross-section were spin-coated with gold and observed by SEM.

Hoechst 33 528 staining was used to observe the cells nuclei of the seeded cells on the scaffolds after 6 days of culture. Samples were washed with PBS and fixed in a 4% paraformaldehyde for 30 minutes at room temperature. After that, they were permeabilized with 0.2% (v/v) Triton X-100 for 15 minutes, followed by washing with PBS. 2 μg mL^{-1} Hoechst 33 528 (343-07961, Dojindo) was added into the fixed sample and kept for 15 minutes at room temperature. For staining of F-actin, Alexa Fluor 488 Phalloidin (Life Technologies) was diluted in PBS with a ratio of 1 : 40 and incubated for 40 minutes. During the incubation, samples in well plates were covered with aluminium foil to avoid light. The stained samples were washed with PBS and observed by fluorescence microscope (Olympus, Japan).

Life/dead staining was used to check the viability of the cells after 1, 4, and 6 days of culture using calcein-AM and propidium iodide staining reagents (Cell-stain Double Staining Kit, Dojindo, Japan). Samples were washed with PBS and incubated in the staining solution for 15 minutes. During the incubation, samples in well plates were covered with aluminum foil to avoid light. Stained samples were analyzed by fluorescence microscope (Olympus, Japan).

Alizarin red S and alkaline phosphatase (ALP) staining were performed on the hMSCs seeded on the scaffold after 7 days of culture. Samples were washed with PBS three times before being fixed in the 4% paraformaldehyde for 10 minutes at room temperature. Afterward, fixed scaffolds were washed with PBS two times and then stained with the staining solution for 10 minutes at room temperature. During the staining process, the sample well plates were covered with aluminum foil to avoid the interference of the light. The staining solution of ALP contains 0.1% fast blue RR salt and 0.1% naphthol AS-MX phosphate, which is diluted in 56 mM 2-amino-2-methyl-1,3-propanediol solution (pH = 9.9). Meanwhile, the alizarin red S staining solution contains 0.5% alizarin red S in PBS solution. The stained samples were then washed with PBS three times and sectioned with a blade to obtain the vertical cross-section. An optimal microscope was used to observe the sectioned samples.

3 Results and discussion

3.1 Exploration of 3D-printed ice

The Aerojet dispenser 3D printer, which utilizes air pressure to eject water through a nozzle and form a different pattern on the

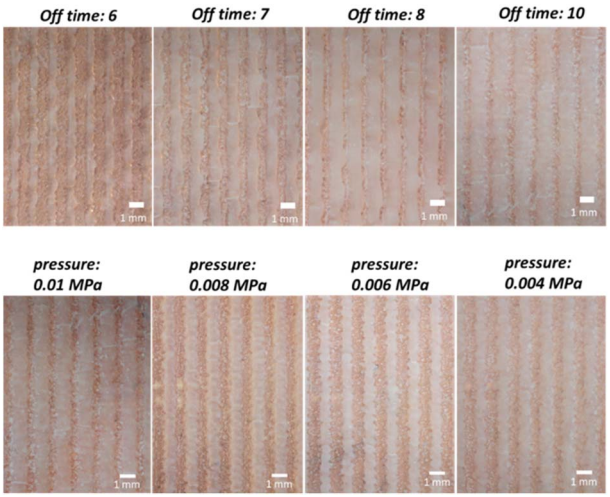

Fig. 1 Formation of 3D printed ice on a frozen copper plate covered by PFA film at different printing settings.

surface of the scaffolds was used. The resolution of the Aerojet 3D printing is essential to form the pattern precisely. Therefore, some parameters during printing including the off time (time interval between the jetting of two water droplets) and air pressure were explored and controlled to obtain a high resolution and stable jetting of ultra-pure water forming 3D frozen printed ice as shown in Fig. 1.

Ultrapure waters were dropped onto a frozen copper plate, which was covered by hydrophobic polyfluoroalkoxy (PFA) film. The use of PFA film was important to provide a good surface tension between water and surface, thus forming a good droplet placement. A simple line pattern was prepared by SHOT mini connected to the jetting machine with a controllable on-time, number of layers, and printing speed. Meanwhile, the off time and air pressure was controlled by the air controller connected to the jetting machine. The line pattern was selected during the optimization of the printing setting.

The printed line width and the gap were optimized by calculating the results using Image-J software. Off time was varied at 6, 7, 8, and 10 ms resulting in the line width (μm) of 531 ± 23, 748 ± 19, 919 ± 40, and 965 ± 13, respectively, and line gap (μm) of 727 ± 50, 548 ± 86, 332 ± 49, and 319 ± 11, respectively. Those results showed that off-time affected the width size of the printed ice, which also affected the line gap. The lower-off time resulted in a fast-printing process with a smaller width of the ice line (higher resolution). Meanwhile, below 6 off time, the formed line was disconnected. Air pressure (MPa) was varied at 0.01, 0.008, 0.006, and 0.004 resulting in the line width (μm) of 1152 ± 41, 851 ± 76, 719 ± 48, and 697 ± 78, respectively, and line gap (μm) of 375 ± 25, 603 ± 32, 681 ± 47, and 736 ± 42, respectively. The air pressure affected the width size of the ice line, with higher air pressure resulting in a larger width of the ice line. This means that lower air pressure could increase the resolution of the printed ice, however, if the pressure is too low, no water droplets will be formed.

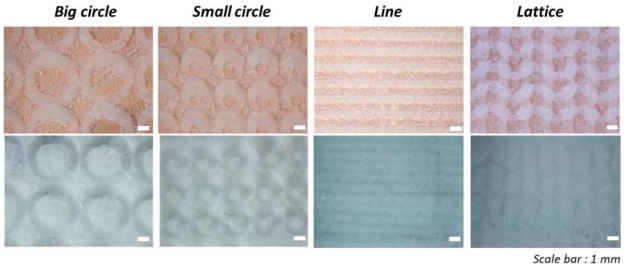

Fig. 2 Formation of printed ice at different designs of pattern on top of the frozen copper plate (top row) and porous gelatin scaffold at different designs of a surface pattern after freeze-drying (bottom row).

3.2 Formation of scaffold with different surface patterns

SHOT Mini, which was used to draw the pattern can be utilized to form lines (*X* and *Y* direction), circles, and curves. Therefore, several patterns including big circles, small circles, horizontal lines, and lattices could be prepared. By using printing conditions of 40 mm s^{-1} printing speed, 3 number of layers, 0.006 MPa air pressure, and 8 ms off time, ultrapure water was jetted onto a frozen copper plate wrapped with PFA film and forming a different pattern of printed ice as shown in Fig. 2 (upper row). The mixture of gelatin/ice particulates was added onto the printed ice and then after the lyophilization, the scaffold with different surface patterns was formed (Fig. 2 (bottom row)).

3.3 HUVEC viability and distribution on the scaffold with different surface patterns

Using the optimum printing setting of 40 mm s^{-1} printing speed, 3 layers, 0.006 MPa air pressure, and 8 ms off time, the different pattern of big circle, small circle, line, and lattice was obtained on the surface of scaffolds. The topographical structure especially at the micro/nanoscale affects the behaviour of HUVECs and plays an essential role in enhancing their performance on the biological function. HUVECs were seeded onto the scaffold with different surface patterns and cultured for 1, 4, and 6 days. In comparison, the control gelatin scaffold without surface pattern and ice particulates was prepared with the same conditions of lyophilization, crosslinking, and sterilization. Live/dead staining was done to analyze the cells' viability after different culture times as shown in Fig. 3(A–C). The staining showed that most of the HUVECs were alive (green fluorescence) and few were dead (red fluorescence) in the scaffold. These results showed that the viability of HUVECs cultured on the scaffold was high. After 1 day of culture, the cell density on all samples was similar showing that different patterns did not affect the initial attachment of HUVECs. However, after the increase of culture time, the cells' density on the big circle, line, and lattice pattern showed more than the small circle pattern and control samples.

Hoechst 33 528 staining was performed to analyze the cell nuclei of the HUVECs cultured on the scaffold after 6 days as shown in Fig. 3(D). These nuclei staining showed the HUVECs alignment, which was affected by the surface pattern.

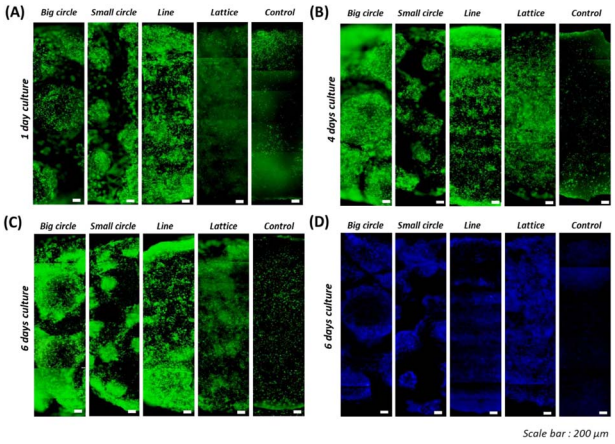

Fig. 3 Live/dead staining of HUVECs seeded on the scaffolds with different surface pattern after (A) 1 day of culture, (B) 4 days of culture, (C) 6 days of culture, and (D) nucleus staining using Hoechst 33 528 after 6 days of culture.

Compared to the control ones, the porous scaffold prepared by ice particulates showed homogeneous cell distribution. More cells were spotted on the porous scaffold. The line and lattice surface of the scaffold, which had a smaller gap and size compared to the circle surface of the scaffold showed homogeneous cell distribution.[13]

F-actin staining was conducted to evaluate the elongation and spreading of HUVECs on different patterns of scaffolds' surface.[12] Fig. 4 shows that HUVECs tend to elongate more and spread less on the patterned porous scaffolds compared to the control scaffolds. It was because the porous construct disrupted the surface geometry.[24] Especially on the line pattern, cell elongation follows the direction of the line pattern. Circle patterns with a bigger size showed less effect on the cell's morphology even though cell has receptive ability to a broad spectrum of size from macro to molecular level.[25] The lattice patterns influenced the volume fraction, which affected the mechanical properties.[26] Higher volume fraction on the lattice pattern provided a larger cell area compared to the other samples. Meanwhile, on the control scaffold, cells showed random orientation and maintained a large spreading. This result has a similar performance to the previous study, which investigated the HUVECs' behaviour on the patterned silk fibroin films.[13] Their results discovered that the orientation and alignment of HUVECs are similarly impacted by grafting of different diameters and the same depth. However, each type of cell will react differently to topographic cues, and the shape, size, depths, and other characteristics should be controlled to guide the cells' behaviour. A similar result was reported on the aligned nanofiber samples, which showed a random orientation on un-patterned nanofiber.[12]

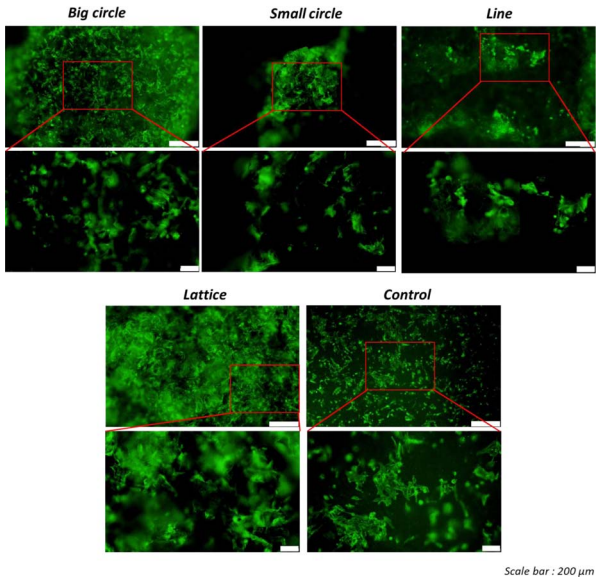

Fig. 4 F-actin staining using phalloidin of HUVECs seeded on the scaffolds with different surface patterns after 6 days of culture. The red square indicates the magnification area.

3.4 Formation of 3D composite sandwich scaffold with patterned surface and interconnected porous structure

After freeze-drying, the 3D composite sandwich scaffold was punched into a disc as shown in Fig. 5. A sandwich construct by putting the PLGA mesh at the center of a gelatin/nano-silica porous scaffold was reported to have improved mechanical properties.[19,27] The PLGA mesh serves as the structural framework of the scaffold, while the gelatin/nano-silica component facilitates cell accommodation.[27] The interaction between gelatin and nano-silica in composite scaffolds occurs primarily through hydrogen bonding between silanol groups (Si–OH) on the nano-silica and amino or carboxyl group in the gelatin chains.[28] As the matrix formulation, gelatin 4% with 70% ice particulates was chosen as the optimum concentration, which facilitated the effective cell seeding and homogeneous ECM formation through scaffold based on the result from previously reported work by Shangwu Chen, *et al.*[29] Their result showed that high content of ice particulates (≥70%) exhibited an open and well-interconnected pore network, which enabled uniform cell distribution. In contrast, scaffold prepared with lower ice particulates ratio exhibited limited pore interconnectivity,

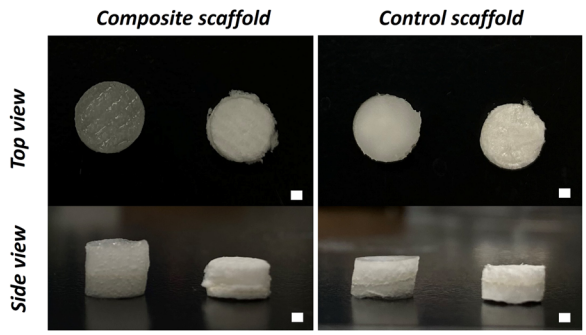

Fig. 5 Appearance of the disc scaffold after water immersion (left column) and before water immersion (right column) during porosity measurement. Scale bar = 1 mm.

resulting in limited cell penetration. Previous works had explored the use of these gelatin/ice particulates for different biomedical applications.[30–33] As comparison, the control scaffold of gelatin/nano-silica/PLGA was prepared without surface pattern and ice particulates. Both composite scaffold and control scaffold in dry and hydrated states are shown in Fig. 5. The porosity of the composite and control scaffolds was calculated using eqn (1) resulted in the porosity of 99.26 ± 1.00 μm and 97.19 ± 0.22 μm, respectively. The porous structure of the composite scaffold showed higher porosity compared to the control scaffold. More water can be absorbed onto the composite scaffold, which is beneficial for cell seeding and the transfer of nutrients during culture.

The stability of hydrated scaffold after the water immersion is correlated with the covalent crosslink using EDC/NHS as the chemical crosslinker. EDC (1-ethyl-e-(3-dimethylaminopropyl) carbodiimide) activates carboxyl groups, enabling its conversion into an NHS-activated intermediate upon reaction with NHS, with urea as a by-product. This intermediate then reacts with a free amine group, resulting in the formation of a stable amide bond that serves as a crosslink between polymer chain.[34]

3.5 Morphology and pore size

SEM analysis was performed to check the morphology and microstructures of the composite and control scaffolds as shown in Fig. 6. The surface images showed that the composite scaffold has open and interconnected pores with a line pattern. Meanwhile, the control scaffold has a skin layer and closed surface pores. The calculation of pores size using image-J software resulted in the line pattern of the composite scaffold's surface with a width of 534 ± 49 μm and a gap of 365 ± 28 μm. The pores were interconnected with a size of interconnected pores of 34 ± 6 μm.

The 3D-printed ice line could control the open pores on the surface of the scaffold, which is beneficial for the cells' penetration and distribution. The depth of the line well of the composite scaffold had the size of 146 ± 17 μm, which can be controlled by adjusting the number of layers of 3D-printed ice. Besides the depth, the width and gap of the line pattern can be adjusted by setting the input on the Aerojet dispenser for 3D-printed ice formation. Previous works reported different sizes and gaps that can be achieved by this method and analyzed its influence on cells.[15,16]

The horizontal and vertical cross-section images showed that both the composite and control scaffold had a spherical large pore. However, the composite scaffold showed a homogeneous structure with interconnected pores. Meanwhile, the control scaffold showed random pores with minimum interconnected pores. The large pores of the composite scaffold were 164 ± 25 μm and the interconnected pores were 36 ± 10 μm. The free ice particulates could control the large pores size of the scaffolds, and the new ice crystals that were formed during the freezing process became the replica of the interconnected pores. Some previous studies have explored the use of ice particulates as porogen materials to control the porous structure of scaffolds.[35–38] The pore size of scaffold affected compressive

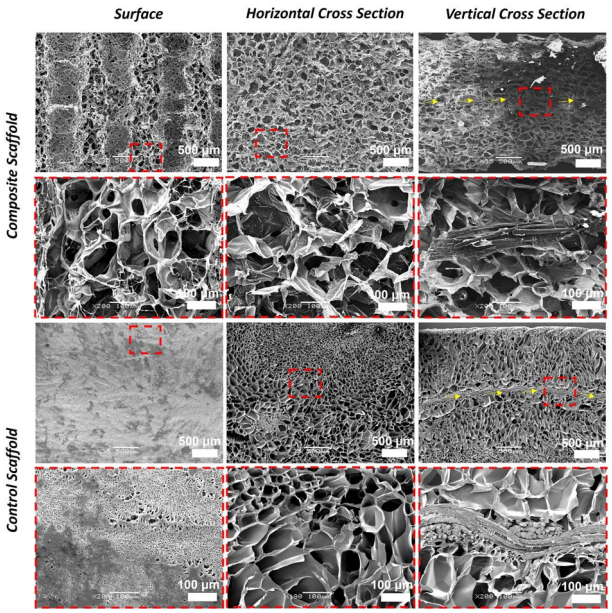

Fig. 6 SEM images of 3D composite sandwich scaffold and control scaffold at low magnification (upper row) and high magnification (lower row). The red dashed squares, yellow arrows, blue circles, and green circles indicate the magnification region, PLGA mesh, large pores, and interconnected pores, respectively.

modulus, which resulting in higher tissue formed in the scaffold.[37] Previous research studied the effect of different ice particulates size using four varied sizes, *e.g.* 150–250 μm, 250–355 μm, 355–425 μm, and 425–500 μm. Their results showed that the highest compressive modulus of cartilage-like tissue was obtained using 150–250 μm ice particulates. That can be explained by the homogeneous cell distribution, where the smaller pores facilitated more efficient cell infiltration compared to the larger pores.[39] In addition, another research studied the effects of gelatin:ice particulates ratio and showed that the compression modulus of scaffold prepared by ice particulates was more uniform and controllable than the control scaffold prepared without the ice particulates. The presence of uniformly arranged and densely packed pores contributed to the mechanical reinforcement of the scaffold.[38] Meanwhile, the control scaffolds prepared without ice particulates exhibited a non-uniform porous architecture and anisotropic compressive modulus, indicating variability in mechanical performance depending on the direction of compression.[29]

The vertical cross-section images also showed that PLGA knitted mesh was integrated well with the gelatin/nano-silica both on the composite and control scaffold. The integration of PLGA as a supportive skeleton within the scaffold provides sufficient mechanical strength to allow fixation during suturing for the clinical application. This is beneficial to secure the graft at the target site, which is still remains a significant challenge, particularly when the scaffold materials is mechanically weak, such as on the gelatin-based construct.[27] Our previous conducted research showed that PLGA improved the tensile

strength of the 3D composite sandwich scaffold.[19] These findings highlight the importance of both material composition and pore structure in achieving mechanically stable scaffolds suitable for load-bearing tissue regeneration.

3.6 hMSCs attachment on the 3D composite sandwich scaffolds with patterned surface and interconnected porous structure

Cells attachment and morphology after 1 day of culture were analyzed using SEM as presented in Fig. 7. It showed the hMSCs attachment on both surfaces of the scaffolds. The surface image presented that the cells were merged and formed a cellular layer.[40] Meanwhile, some of the cells were migrated inside the scaffolds as shown in the horizontal and vertical cross-section images. The vertical cross-section on the centre of the scaffold showed that more cells were observed on the composite scaffold compared to the control scaffolds. The interconnected porous structure and open pores contributed to cell penetration on the composite scaffold.

3.7 hMSCs viability, ALP, and alizarin red S analysis on the 3D composite scaffolds with patterned surface and interconnected porous structure

Live/dead staining was performed to check the cell viability on the scaffolds after 7 days of culture as shown in Fig. 8(A). The surface images showed that hMSC were alive and attached both on the composite and control scaffolds. Meanwhile, the vertical cross-section showed that more cells were spotted inside the centre of composite scaffold compared to control scaffold. At the control scaffold, most of the cells were attached to the surface and fewer cells were spotted at the centre of control scaffolds.

Hoechst 33 528 staining was performed to stain the cell nuclei, and phalloidin staining was conducted to stain F-actin of hMSCs seeded on the scaffold after 7 days of culture (Fig. 8(B)). The surface images showed that cells were distributed both on the surface of composite and control scaffolds. There was more void in the centre of control scaffolds without any cells. Besides the homogeneous cell distribution due to the interconnected porous geometry on the composite scaffolds, the addition of nano-silica encouraged cell proliferation and

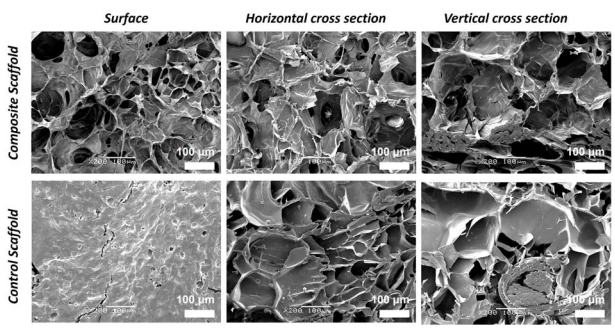

Fig. 7 SEM images of hMSCs seeded on the 3D composite and control scaffold after 1 day of culture.

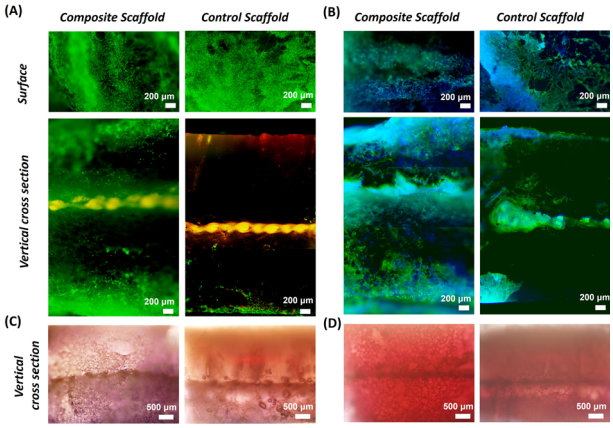

Fig. 8 (A) Live/dead staining, (B) nucleus staining by Hoechst 33 528 and F-actin staining by phalloidin, (C) ALP staining, and (D) Alizarin red S staining after 7 day culture of hMSCs seeded on the 3D composite and control scaffold.

improved the bioactivity and cellular behaviour.[41] Those lead to strong alkaline phosphatase and alizarin red S staining on the composite scaffolds as shown in Fig. 8(C and D), which indicates the osteogenic potential. The stronger ALP and Alizarin red S staining was observed on the composite scaffold, compared to the control scaffold. ALP provides an important function to initiate matrix mineralization, which is beneficial for bone tissue regeneration.[42] Meanwhile, the alizarin red S revealed the existence of a hydroxyapatite layer and evaluated the level of mineralization.[43] The dark red spots on the staining showed calcium deposition, which indicates enhanced mineralization inside the scaffolds, which is stimulated by bioactive nano-silica.[44]

Besides mineralization, vascularization plays a critical role in bone tissue regeneration, which can be assessed by the angionenic promotion. Although direct angiogenic assays were not included on this manuscripts, the early assessment of cells proliferation of HUVECs on the patterned scaffold showed enhanced cell adhesion compared to the un-pattered control scaffold. In addition, the previous studies have demonstrated that the nano-silica inclusion on the gelatin scaffold enhances angiogenic responses, including upregulated VEGF expression and improved endothelial network formation.[45]

4 Conclusions

3D composite gelatin/nano-silica/PLGA scaffold with surface patterning and interconnected porous architecture was successfully fabricated by nozzle-based Aerojet dispenser 3D printing and freeze-drying method. Exploration of the printing process of water onto frozen substrate was performed to obtain high-resolution and stable printed ice as fugitive ink to form a patterned surface. Different patterns including the big circle, small circle, line, and lattice pattern of porous gelatin scaffold were fabricated using the optimum printing condition. *In vitro* culture of HUVECs onto a surface patterned scaffold was conducted to analyze the cells' behaviour and orientation. The

addition of printed ice and ice particulates could form a homogeneous interconnected pores structure in the matrix and controlled orientation surface pores. hMSCs were seeded on the 3D composite scaffold and control scaffold prepared by freeze-drying method. The cell attachment, cell viability, and cell distribution on the 3D composite scaffold were higher than the control scaffold due to its porous architecture. The addition of nano-silica showed an improved ALP and Alizarin red S activity, which initiated the matrix mineralization for bone tissue regeneration. Based on the early assessment on this research using *in vitro* analysis on the bone regeneration using hMSC and HUVECS, further *in vivo* analysis needs to be done in the future work to support the study of angiogenesis and osteogenesis in bone tissue formation using this 3D composite scaffold.

Author contributions

Nur R. E. Putri designed and conducted the main experimental work on scaffold fabrication and characterization; Huajian Chen carried out the experiments on the cell's characterization; Naoki Kawazoe contributed on the experimental process and data analysis; Felicity R. A. J. Rose contributed on the supervision; Ricky. D. Wildman contributed to the supervision; Guoping Chen contributed on the supervision and providing the funding. All authors discussed the results and contributed to the writing, reviewing, and revising the manuscript.

Conflicts of interest

The authors declare no conflict of interest.

Data availability

The supporting data for this study are available in the manuscript.

Acknowledgements

This research was partially supported by JSPS KAKENHI Grant Number 24K03289.

References

1 L. Claes, S. Recknagel and A. Ignatius, Fracture healing under healthy and inflammatory conditions, *Nat. Rev. Rheumatol.*, 2012, **8**(3), 133–143, DOI: 10.1038/nrrheum.2012.1.
2 J. A. Cottrell, J. C. Turner, T. L. Arinzeh and J. P. O. Connor, The Biology of Bone and Ligament Healing, *Foot Ankle Clin.*, 2016, **21**, 739–761, DOI: 10.1016/j.fcl.2016.07.017.
3 B. Beamer, C. Hettrich and J. Lane, Vascular Endothelial Growth Factor: An Essential Component of Angiogenesis and Fracture Healing, *HSS J.*, 2015, **6**(June), 85–94, DOI: 10.1007/s11420-009-9129-4.
4 M. Orciani, M. Fini, R. Di Primio and M. Mattioli-Belmonte, Biofabrication and bone tissue regeneration: cell source, approaches, and challenges, *Front. Bioeng. Biotechnol.*, 2017, **5**(MAR), 1–15, DOI: 10.3389/fbioe.2017.00017.
5 F. O'Brien, Biomaterials & scaffolds for tissue engineering, *Mater. Today*, 2011, **14**(3), 88–95, DOI: 10.1016/S1369-7021(11)70058-X.
6 M. I. Santos and R. L. Reis, Vascularization in bone tissue engineering: physiology, current strategies, major hurdles and future challenges, *Macromol. Biosci.*, 2010, **10**(1), 12–27, DOI: 10.1002/mabi.200900107.
7 C. Vyas, R. Pereira, B. Huang, F. Liu, W. Wang and P. Bartolo, Engineering the vasculature with additive manufacturing, *Curr. Opin. Biomed. Eng.*, 2017, **2**, 1–13, DOI: 10.1016/j.cobme.2017.05.008.
8 J. Rouwkema and A. Khademhosseini, Vascularization and Angiogenesis in Tissue Engineering: Beyond Creating Static Networks, *Trends Biotechnol.*, 2016, **34**(9), 733–745, DOI: 10.1016/j.tibtech.2016.03.002.
9 J. Yang, F. R. A. J. Rose, N. Gadegaard and M. R. Alexander, A high-throughput assay of cell-surface interactions using topographical and chemical gradients, *Adv. Mater.*, 2009, **21**(3), 300–304, DOI: 10.1002/adma.200801942.
10 G. Li, X. Zhao, W. Zhao, *et al.*, Porous chitosan scaffolds with surface micropatterning and inner porosity and their effects on Schwann cells, *Biomaterials*, 2014, **35**(30), 8503–8513, DOI: 10.1016/j.biomaterials.2014.05.093.
11 B. J. Papenburg, L. Vogelaar, L. A. M. Bolhuis-versteeg, R. G. H. Lammertink, D. Stamatialis and M. Wessling, One-step fabrication of porous micropatterned scaffolds to control cell behavior, *Biomaterials*, 2009, **28**(2007), 1998–2009, DOI: 10.1016/j.biomaterials.2006.12.023.
12 M. Moffa, A. G. Sciancalepore and L. G. Passione, Combined Nano- and Micro-Scale Topographic Cues for Engineered Vascular Constructs by Electrospinning and Imprinted Micro-Patterns, *Small*, 2014, **10**(12), 2439–2450, DOI: 10.1002/smll.201303179.
13 X. Du, Y. Wang, L. Yuan, Y. Weng, G. Chen and Z. Hu, Guiding the behaviors of human umbilical vein endothelial cells with patterned silk fibroin films, *Colloids Surf., B*, 2014, **122**, 79–84, DOI: 10.1016/j.colsurfb.2014.06.049.
14 G. Li, X. Zhao, W. Zhao, *et al.*, Porous chitosan scaffolds with surface micropatterning and inner porosity and their effects on Schwann cells, *Biomaterials*, 2014, **35**(30), 8503–8513, DOI: 10.1016/j.biomaterials.2014.05.093.
15 S. Chen, T. Nakamoto, N. Kawazoe and G. Chen, Engineering multi-layered skeletal muscle tissue by using 3D microgrooved collagen scaffolds, *Biomaterials*, 2015, **73**, 23–31, DOI: 10.1016/j.biomaterials.2015.09.010.
16 Y. Chen, S. Chen, N. Kawazoe and G. Chen, Promoted Angiogenesis and Osteogenesis by Dexamethasone-loaded Calcium Phosphate Nanoparticles/Collagen Composite Scaffolds with Microgroove Networks, *Sci. Rep.*, 2018, **8**(1), 1–12, DOI: 10.1038/s41598-018-32495-y.
17 T. Kokubo and H. Takadama, How useful is SBF in predicting *in vivo* bone bioactivity?, *Biomaterials*, 2006, **27**(15), 2907–2915, DOI: 10.1016/j.biomaterials.2006.01.017.

18 J. A. Sowjanya, J. Singh, T. Mohita, *et al.*, Biocomposite scaffolds containing chitosan/alginate/nano-silica for bone tissue engineering, *Colloids Surf., B*, 2013, **109**, 294–300, DOI: 10.1016/j.colsurfb.2013.04.006.

19 N. R. Eviana Putri, X. Wang, Y. Chen, X. Li, N. Kawazoe and G. Chen, Preparation of PLGA-collagen hybrid scaffolds with controlled pore structures for cartilage tissue engineering, *Prog. Nat. Sci. Mater. Int.*, 2020, **30**(5), 642–650, DOI: 10.1016/j.pnsc.2020.07.003.

20 E. Choi, D. Kim, D. Kang, *et al.*, 3D-printed gelatin methacrylate (GelMA)/silanated silica scaffold assisted by two-stage cooling system for hard tissue regeneration, *Regen. Biomater.*, 2021, 1–14, DOI: 10.1093/rb/rbab001. Published online.

21 C. V. Rahman, G. Kuhn, L. J. White, *et al.*, PLGA/PEG-hydrogel composite scaffolds with controllable mechanical properties, *J. Biomed. Mater. Res., Part B*, 2013, **101**(4), 648–655, DOI: 10.1002/jbm.b.32867.

22 H. Zreiqat, Y. Ramaswamy, C. Wu, *et al.*, The incorporation of strontium and zinc into a calcium-silicon ceramic for bone tissue engineering, *Biomaterials*, 2010, **31**(12), 3175–3184, DOI: 10.1016/j.biomaterials.2010.01.024.

23 T. T. Nge, M. Nogi, H. Yano and J. Sugiyama, Microstructure and mechanical properties of bacterial cellulose/chitosan porous scaffold, *Cellulose*, 2010, **17**(2), 349–363, DOI: 10.1007/s10570-009-9394-x.

24 S. M. Casillo, A. P. Peredo, S. J. Perry, H. H. Chung and T. R. Gaborski, Membrane Pore Spacing Can Modulate Endothelial Cell – Substrate and Cell – Cell Interactions, *ACS Biomater. Sci. Eng.*, 2017, **3**, 243–248, DOI: 10.1021/acsbiomaterials.7b00055.

25 J. Mitra, G. Tripathi, A. Sharma and B. Basu, Scaffolds for bone tissue engineering: Role of surface patterning on osteoblast response, *RSC Adv.*, 2013, **3**(28), 11073–11094, DOI: 10.1039/c3ra23315d.

26 I. Maskery, A. O. Aremu, L. Parry, R. D. Wildman, C. J. Tuck and I. A. Ashcroft, Effective design and simulation of surface-based lattice structures featuring volume fraction and cell type grading, *Mater. Des.*, 2018, **155**, 220–232, DOI: 10.1016/j.matdes.2018.05.058.

27 W. Dai, N. Kawazoe, X. Lin, J. Dong and G. Chen, The influence of structural design of PLGA/collagen hybrid scaffolds in cartilage tissue engineering, *Biomaterials*, 2010, **31**(8), 2141–2152, DOI: 10.1016/j.biomaterials.2009.11.070.

28 M. Ghanbari, M. Salavati-Niasari, F. Mohandes, B. Dolatyar and B. Zeynali, In vitro study of alginate-gelatin scaffolds incorporated with silica NPs as injectable, biodegradable hydrogels, *RSC Adv.*, 2021, **11**(27), 16688–16697, DOI: 10.1039/d1ra02744a.

29 S. Chen, Q. Zhang, T. Nakamoto, N. Kawazoe and G. Chen, Gelatin Scaffolds with Controlled Pore Structure and Mechanical Property for Cartilage Tissue Engineering, *Tissue Eng., Part C*, 2015, 1–29, DOI: 10.1089/ten.TEC.2015.0281.

30 J. Zhang, J. Li, S. Chen, N. Kawazoe and G. Chen, Preparation of gelatin/Fe_3O_4 composite scaffolds for enhanced and repeatable cancer cell ablation, *J. Mater. Chem. B*, 2016, **4**(34), 5664–5672, DOI: 10.1039/c6tb01543c.

31 X. Wang, J. Zhang, J. Li, *et al.*, Bifunctional scaffolds for the photothermal therapy of breast tumor cells and adipose tissue regeneration, *J. Mater. Chem. B*, 2018, **6**(46), 7728–7736, DOI: 10.1039/c8tb02325e.

32 J. Zhang, J. Li, N. Kawazoe and G. Chen, Composite scaffolds of gelatin and gold nanoparticles with tunable size and shape for photothermal cancer therapy, *J. Mater. Chem. B*, 2017, **5**(2), 245–253, DOI: 10.1039/c6tb02872a.

33 J. Zhang, J. Li, X. Wang, N. Kawazoe and G. Chen, Targeting ligand-functionalized photothermal scaffolds for cancer cell capture and: *in situ* ablation, *Biomater. Sci.*, 2017, **5**(11), 2276–2284, DOI: 10.1039/c7bm00639j.

34 M. G. Haugh, C. M. Murphy, R. C. McKiernan, C. Altenbuchner and F. J. O'Brien, Crosslinking and Mechanical Properties Significantly Influence Cell Attachment, Proliferation, and Migration Within Collagen Glycosaminoglycan Scaffolds, *Tissue Eng., Part A*, 2011, **17**(9–10), 1201–1208, DOI: 10.1089/ten.tea.2010.0590.

35 Y. G. Ko, N. Kawazoe, T. Tateishi and G. Chen, Preparation of Novel Collagen Sponges Using an Ice Particulate Template, *J. Bioact. Compat. Polym.*, 2010, **25**(4), 360–373, DOI: 10.1177/0883911510370002.

36 Q. Zhang, H. Lu, N. Kawazoe and G. Chen, Preparation of collagen porous scaffolds with a gradient pore size structure using ice particulates, *Mater. Lett.*, 2013, **107**, 280–283, DOI: 10.1016/j.matlet.2013.05.070.

37 Q. Zhang, H. Lu, N. Kawazoe and G. Chen, Pore size effect of collagen scaffolds on cartilage regeneration, *Acta Biomater.*, 2014, **10**(5), 2005–2013, DOI: 10.1016/j.actbio.2013.12.042.

38 Q. Zhang, H. Lu, N. Kawazoe and G. Chen, Preparation of collagen scaffolds with controlled pore structures and improved mechanical property for cartilage tissue engineering, *J. Bioact. Compat. Polym.*, 2013, **28**(5), 426–438, DOI: 10.1177/0883911513494620.

39 H. Stenhamre, U. Nannmark, A. Lindahl, P. Gateholm and M. Brittberg, Influence of pore size on the redifferentiation potential of human articular chondrocytes in poly(urethane urea) scaffolds, *J. Tissue Eng. Regener. Med.*, 2011, **5**, 578–588, DOI: 10.1002/term.

40 K. G. Jain, S. Mohanty, A. R. Ray, R. Malhotra and B. Airan, Culture & differentiation of mesenchymal stem cell into osteoblast on degradable biomedical composite scaffold: *in vitro* study, *Indian J. Med. Res.*, 2015, **142**(6), 747–758, DOI: 10.4103/0971-5916.174568.

41 K. C. Kavya, R. Jayakumar, S. Nair and K. P. Chennazhi, Fabrication and characterization of chitosan/gelatin/*n*SiO_2 composite scaffold for bone tissue engineering, *Int. J. Biol. Macromol.*, 2013, **59**, 255–263, DOI: 10.1016/j.ijbiomac.2013.04.023.

42 A. Ehara, K. Ogata, S. Imazato, S. Ebisu, T. Nakano and Y. Umakoshi, Effects of α-TCP and TetCP on MC3T3-E1 proliferation, differentiation and mineralization, *Biomaterials*, 2003, **24**(5), 831–836, DOI: 10.1016/S0142-9612(02)00411-8.

43 N. Khatami, A. B. Khoshfetrat, M. Khaksar, A. R. N. Zamani and R. Rahbarghazi, Collagen-alginate-nano-silica microspheres improved the osteogenic potential of human osteoblast-like MG-63 cells, *J. Cell. Biochem.*, 2019, **120**(9), 15069–15082, DOI: **10.1002/jcb.28768**.

44 G. R. Beck, S. W. Ha, C. E. Camalier, *et al.*, Bioactive silica-based nanoparticles stimulate bone-forming osteoblasts, suppress bone-resorbing osteoclasts, and enhance bone mineral density *in vivo*, *Nanomedicine Nanotechnology, Biol Med.*, 2012, **8**(6), 793–803, DOI: **10.1016/j.nano.2011.11.003**.

45 C. C. Ho, S. C. Huang, C. K. Wei and S. J. Ding, *In vitro* degradation and angiogenesis of the porous calcium silicate–gelatin composite scaffold, *J. Mater. Chem. B*, 2016, **4**(3), 505–512, DOI: **10.1039/c5tb02401c**.